minerals

MDPI

Article

Utilisation of Biosilica as Active Silica Source for Metakaolin-Based Geopolymers

Haozhe Guo [1,2,3], Zhihao Huang [4], Thammaros Pantongsuk [4], Ting Yu [5,*], Baifa Zhang [5], Jinghan Luo [4] and Peng Yuan [5]

[1] Institute of Resources Utilization and Rare Earth Development, Guangdong Academy of Sciences, Guangzhou 510650, China; guohaozhe@grre.gd.cn
[2] State Key Laboratory of Rare Metals Separation and Comprehensive Utilization, Guangzhou 510650, China
[3] Guangdong Provincial Key Laboratory of Development and Comprehensive Utilization of Mineral Resources, Guangzhou 510650, China
[4] CAS Key Laboratory of Mineralogy and Metallogeny/Guangdong Provincial Key Laboratory of Mineral Physics and Materials, Guangzhou Institute of Geochemistry, Chinese Academy of Sciences, Guangzhou 510640, China; huangzhihao_gig24@163.com (Z.H.); thammaros@gig.ac.cn (T.P.); luojinghan22@mails.ucas.ac.cn (J.L.)
[5] School of Environmental Science and Engineering, Guangdong University of Technology, Guangzhou 510006, China; zhangbaifa@gdut.edu.cn (B.Z.); yuanpeng@gdut.edu.cn (P.Y.)
* Correspondence: yuting@gig.ac.cn

Abstract: This study explores the potential of biosilica including diatom and diatomaceous earth as alternative silica sources for metakaolin-based geopolymers. Diatomaceous earth, composed of fossilised diatom frustules rich in amorphous silica, and diatoms, a sustainable source of renewable biosilica, are investigated for their effectiveness in enhancing geopolymer properties. Through detailed analyses including FTIR, XRD, and SEM, the study evaluates the impact of these biosilica sources on geopolymer compressive strength and microstructure, comparing them with conventional sodium silicate. Results show that diatoms exhibit significant promise, achieving 28-day strength up to 17.9 MPa at a 30% mass fraction, while diatomaceous earth reaches 26.2 MPa at a 50% addition rate, demonstrating their potential as active silica sources. Furthermore, the study elucidates the role of organic matter in biosilica on geopolymerisation, highlighting its influence on active silica release and the strength performance of products. This study proposes a novel pathway to enhance the sustainability of geopolymers through the utilisation of biosilica from diatoms, contributing to advancements in eco-efficient construction materials.

Keywords: geopolymers; diatom; diatomite; biosilica; sustainable materials

check for updates

Citation: Guo, H.; Huang, Z.; Pantongsuk, T.; Yu, T.; Zhang, B.; Luo, J.; Yuan, P. Utilisation of Biosilica as Active Silica Source for Metakaolin-Based Geopolymers. *Minerals* **2024**, *14*, 816. https://doi.org/10.3390/min14080816

Academic Editor: Javier Sánchez-España

Received: 20 July 2024
Revised: 8 August 2024
Accepted: 10 August 2024
Published: 12 August 2024

Copyright: © 2024 by the authors. Licensee MDPI, Basel, Switzerland. This article is an open access article distributed under the terms and conditions of the Creative Commons Attribution (CC BY) license (https://creativecommons.org/licenses/by/4.0/).

1. Introduction

Geopolymers have emerged as a promising eco-friendly cementitious material due to their lower energy requirements and reduced CO_2 emissions during production [1,2]. These materials are synthesised from aluminosilicates, such as low-temperature calcined clay and solid wastes (e.g., fly ash and slag), under the influence of alkaline or acidic activators [3–6], offering superior mechanical strength, thermal resistance, and chemical durability [7,8]. In particular, solid-waste-based geopolymers stand in contrast to the energy-intensive production processes of cement and have suited practical applications in infrastructure development [9,10]. In addition, metakaolin, derived from calcining kaolinite at temperatures below 650–800 °C, is the most widely utilised natural raw material for geopolymers [11]. Although metakaolin-based geopolymers exhibit superior properties compared to solid-waste-based ones, they are not a viable replacement for cement due to the high water requirement and propensity for cracking, but still have promising applications in binders [11], coatings [12], and tiles [13]. Consequently, further research and development is required to advance this material towards practical applications.

Optimising the silica/alumina (SiO_2/Al_2O_3) molar ratio is crucial for enhancing the performance of metakaolin-based geopolymers [11]. Studies indicate that incorporating active silica sources can improve material properties, affecting factors such as setting time and compressive strength [14]. Current methods often rely on sodium silicate. Despite the effectiveness of this approach, the production process of sodium silicate employs high temperatures (up to 1300 °C) and emits significant CO_2 [15], undermining the low-carbon benefits of geopolymers and increasing production costs. Therefore, exploring eco-efficient and sustainable alternatives to sodium silicate for regulating the SiO_2/Al_2O_3 ratio in geopolymers is essential.

Diatomaceous earth is a sedimentary rock composed of fossilised frustules of diatoms, which are rich in amorphous silica (SiO_2) [16]. It possesses favourable physical and chemical properties including high surface area, high permeability, and low thermal conductivity [17,18]. In recent years, diatomaceous earth has been recognised for its pozzolanic activity, positioning it as a potential supplementary cementitious material (SCM) supported by various studies [19–22]. However, diatoms, the biological source of diatomaceous earth, have not been explored as silica supplements in geopolymer synthesis, although the fresh frustules of diatoms share an identical chemical composition with fossilised ones of diatomaceous earth [23]. Diatoms are a renewable natural material. They could be harvested in large quantities with minimal energy and material inputs [24], which makes them more eco-effective than diatomaceous earth when used as geopolymer preparations. Moreover, both diatoms and diatomaceous earth originate from biosilica sources, containing significant organic matter, including polysaccharides and amino acids within their frustules [25,26], the implications of which on their chemical behaviour during geopolymerisation remain unclear.

This study aims to investigate biosilica as the active silica source in metakaolin-based geopolymers. Specifically, it examined the impact of frustules in diatom and diatomaceous earth on geopolymer compressive strength under varying mass fractions, and compared results with geopolymers prepared using sodium silicate. Through Fourier-transform infrared spectroscopy (FTIR), X-ray diffraction (XRD), and field emission scanning electron microscopy (FESEM) analyses, the study assessed compositional and structural differences in geopolymer products before and after organic matter removal from diatom and diatomaceous earth. The findings aim to elucidate the unique contributions of diatomite and diatoms to geopolymer synthesis and the influence of organic matter on material properties.

2. Materials and Methods

2.1. Materials

In this study, the performance of commercial sodium silicate solution references was compared to that of systems utilising diatoms (DB) and diatomaceous earth (DE) as the active silica source of metakaolin-based geopolymers. The DB was purchased under the brand name Zaomeikang Biotechnology Co. from Tianjin, China, while the DE was sourced from Tongliao in Inner Mongolia, China. The chemical compositions of the raw materials were analysed by a Shimadzu XRF-1800 X-ray fluorescence (XRF) spectrometer (Shimadzu, Kyoto, Japan) using wavelength-dispersive spectroscopy. The results are presented in Table 1. The DB had a similar SiO_2 content but a higher Al_2O_3 content than the DE. The high-level loss on ignition (LOI) of both biosilica sources was considered to be rich in organic matter [26,27]. Calcination treatment (750 °C, 3 h) was conducted on DE and DB to obtain the organic-matter-free diatomaceous earth (CDE) and diatoms (CDB).

The kaolin, comprising 95 wt% of kaolinite, was sourced from Maomin in Guangdong, China. The metakaolin was obtained by calcining the kaolin at the temperature of 750 °C in a muffle furnace for 2 h [28]. The main component of metakaolin was aluminosilicate, with a SiO_2/Al_2O_3 molar ratio of 2.0.

Two types of activators were employed for the preparation of geopolymers. One of these was the solution of 10 mol/L sodium hydroxide (10 M NaOH). The preparation of this activator involved the dissolution of NaOH pellets (analytical reagent, purity 96%) in

deionised water in a proportionate manner until a clear solution was obtained. The other activator was prepared by dissolving NaOH pellets in sodium silicate solution. It was recommended that each kind of activator be cooled for a minimum of 24 h after preparation, with the container kept sealed to minimise atmospheric carbonation.

Table 1. Chemical compositions of the raw materials (wt%).

Materials	SiO_2	Al_2O_3	CaO	Fe_2O_3	K_2O	Na_2O	MgO	TiO_2	Others	LOI
DB	64.00	15.95	0.39	5.14	2.15	0.63	0.71	0.82	0.26	9.95
DE	67.90	4.92	0.41	2.67	0.88	0.56	0.60	0.21	1.11	20.74
Metakaolin	52.54	43.50	0.05	0.76	0.74	0.14	0.12	0.56	0.33	1.26
Sodium silicate	26.50	–	–	–	–	8.50	–	–	65.00	–

2.2. Preparation of Geopolymers

Geopolymer pastes with different active silica sources were cast using a cement mixer according to the design presented in Table 2. In the case of preparing geopolymers with sodium silicate as the active silica source, the activators were mixed directly with metakaolin. When the DB, DE, and their calcined products (CDB and CDE) were employed, they needed to be pre-blended with the activators of 10 M NaOH by mechanical stirring for 24 h to ensure the dissolution of active silica. The resulting mixture was then combined with metakaolin in the bowl.

Table 2. Mix design for geopolymers. The liquid-to-solid (L/S) ratio was defined as the ratio between the mass of the activators (10 M NaOH solution or sodium silicate with dissolved NaOH) and the total mass of the solid phase.

Solid Raw Materials				Activator	Molar Ratio		L/S	Sample
Main Source	wt%	Silica Source	wt%		SiO_2/Al_2O_3	Na_2O/Al_2O_3		
Metakaolin	90.0	DB	10.0	10 M NaOH	2.2	0.6	0.7	G_{B10}
	80.0		20.0		2.5	0.7	0.7	G_{B20}
	70.0		30.0		2.7	0.7	0.7	G_{B30}
	60.0		40.0		3.0	0.8	0.7	G_{B40}
	50.0		50.0		3.3	0.9	0.7	G_{B50}
	70.0	CDB	30.0		2.8	0.8	0.7	G_{CB30}
	90.0	DE	10.0		2.3	0.6	0.6	G_{E10}
	80.0		20.0		2.6	0.7	0.6	G_{E20}
	70.0		30.0		3.0	0.8	0.6	G_{E30}
	60.0		40.0		3.5	0.9	0.6	G_{E40}
	50.0		50.0		4.2	1.1	0.6	G_{E50}
	50.0	CDE	50.0		4.7	0.9	0.6	G_{CE50}
	100.0	–	–	NaOH and sodium silicate solution	2.7	0.8	0.9	$G_{S2.7}$
	100.0	–	–	10 M NaOH	2.0	0.5	1.0	G_{MK}

Upon contact between the activators and metakaolin, the mixer commenced operation at a low speed for 60 s followed by a 90 s interval to wipe pastes adhering to the bowl's interior wall to the centre. Operation then resumed at a high speed for a further 4 min. The resulting paste was then placed into cube-shaped moulds with dimensions of $20 \times 20 \times 20$ mm^3 and vibrated for 1 min to remove the air bubbles. All specimens were stored in an environmental chamber at a fixed temperature of 40 ± 1 °C and relative humidity (RH) of $98 \pm 2\%$, with a plastic wrap cover in place to prevent water loss. After one day, the specimens were unmoulded and left at room temperature until testing. The geopolymers prepared with DB, CDB, DE, and CDE as the active sources were designated as G_B, G_{CB}, G_E, and G_{CE}, respectively. The mass fraction of silica sources in the solid raw materials was indicated at the end of the designation to represent the different groups. To

illustrate, G_{B10} was prepared from solids comprising 10 wt% DB and 90 wt% metakaolin. In addition, G_S was used to name the geopolymers containing sodium silicate, with the designed molar ratio of SiO_2/Al_2O_3 denoting the grouping at the end.

2.3. Characterisation

The compressive strengths of geopolymers were measured by a YAW-300D Computer Control Electronic Compression testing machine (HST Group, Jinan, China), which had a load capacity of 300 kN. The applied load rate on the specimen was 500 N/s. One-way analysis of variance (ANOVA) was employed to ascertain the discrepancies in compressive strengths attributable to the active silica sources, with Tukey's post hoc multiple comparison tests [29].

The specific surface area (S_{BET}) was calculated from the N_2 adsorption data using the Brunauer–Emmett–Teller (BET) method [30]. The nitrogen (N_2) adsorption and desorption isotherms were measured at liquid nitrogen temperature by using the Micromeritics ASAP2020 system. Prior to measurement, all samples were subjected to 12 h of outgassing at 120 °C to eliminate any physically adsorbed water.

The mineral compositions were identified through the analysis of XRD patterns, which were recorded on a Bruker D8 Advance diffractometer utilising Cu-*Kα* radiation (λ = 0.154 nm) and Ni-filtered generated at 40 kV and 40 mA. The scanning range was set to encompass 5° to 70° (2θ), with a step width of 0.02° (2θ).

FTIR tests were conducted on a Bruker VERTEX 70 infrared spectrometer to investigate the chemical environment of the element. The sample was mixed with KBr and then pressed into a transparent slice. The spectrum of the slice was collected in the wavenumber range from 4000 cm^{-1} to 400 cm^{-1} under transmittance mode. A spectral resolution of 4 cm^{-1} was selected, and each spectrum was derived from the average of 60 scans.

Microstructures were identified through the use of FESEM, operated with SU8010 (Hitachi, Tokyo, Japan) at an accelerating voltage of 1.5 kV. The equipped AMETEK energy dispersive X-ray spectrometer (EDS) (Hitachi, Tokyo, Japan) was employed for EDS spot analysis of the micro-component content with a voltage of 15 kV and a current of 20 μA.

3. Results and Discussion

3.1. Compressive Strengths

3.1.1. Influence of Mass Fractions

Figure 1a illustrates the compressive strengths of G_B with varying mass fractions of DB at 7 and 28 days. All specimen groups achieved at least 9.0 MPa at 7 days, with strengths exceeding 12.0 MPa at 28 days. The impact of DB mass fractions on strength was assessed using ANOVA, revealing a significant effect ($p < 0.05$). Tukey's post hoc multiple comparisons (Table 3) further clarified that this effect primarily resulted in statistical differences between the 7-day strengths of G_{B20}, G_{B30}, and G_{B40}, as well as between the 28-day strengths of G_{B10} and G_{B30}. Consequently, the G_{B30} only labelled "a" exhibited significantly higher 7- and 28-day compressive strengths than the other G_B, reaching 15.0 and 17.9 MPa, respectively. This indicates that a 30 wt% addition of DE as an active silica source for metakaolin-based geopolymers is optimal in this study.

Table 3. ANOVA test and Tukey's post hoc test.

Sample		Compressive Strength (MPa)					ANOVA	
		10 wt%	**20 wt%**	**30 wt%**	**40 wt%**	**50 wt%**	**F**	***p***
G_B	7 days	10.6 bc [1]	12.1 b	15.0 a	9.1 c	10.0 bc	15.043	0.000
	28 days	12.4 b	17.2 ab	17.9 a	13.7 ab	13.7 ab	4.871	0.002
G_E	7 days	12.6 c	18.8 b	23.8 a	20.4 b	18.8 b	44.632	0.000
	28 days	10.8 b	23.7 a	24.6 a	25.7 a	26.2 a	85.327	0.000

[1] The groups indicated by a, b, and c exhibited significant differences ($p < 0.05$).

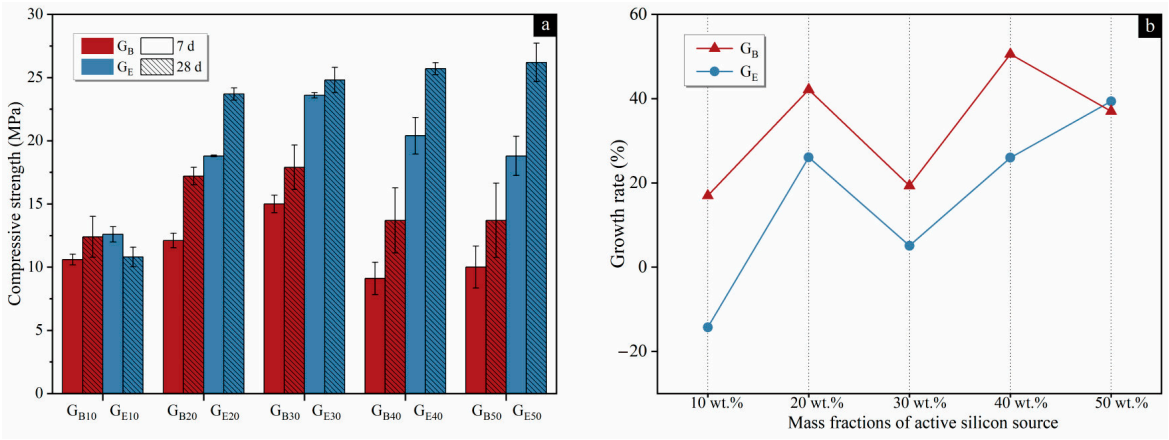


Figure 1. (**a**) The compressive strength of geopolymers at 7 and 28 days with the error bar representing the upper and lower 95% confidence interval; (**b**) The growth rate of compressive strengths between 7 to 28 days.

A series of G_E samples with varying mass fractions of DE (ranging from 10 wt% to 50 wt%) were synthesised and subjected to comparative analysis with G_B. Despite DE's silica content being comparable to DB, the strength of G_E (Figure 1a) consistently surpassed that of G_B across similar mass fractions, except for G_{E10}. G_E exhibited at least a 38% strength increment compared to G_B for each mass fraction level. This enhancement in strength may be attributed to differences in the chemical environment of silica between DB and DE, which will be explored further in the subsequent section.

Based on the results of ANOVA, the mass fraction of DE shows varying effects on the 28-day compressive strength of G_E. There were no significant differences in compressive strength observed among G_{E20}, G_{E30}, G_{E40}, and G_{E50}. Only at a 10 wt% mass fraction of DE did a significant decrease in strength occur. Considering metakaolin as a solid raw material requiring calcination treatment, substituting more DE is beneficial for reducing the carbon footprint associated with metakaolin-based geopolymers. Therefore, the optimal addition of DE is deemed to be 50 wt%. Furthermore, concerning the development of strength over the 7- to 28-day period, both DB and DE exhibit similar effects. Specifically, the maximum 7-day strengths of G_B and G_E were achieved when DB and DE were added at 30 wt%, which was close to or even greater than the other groups of geopolymers' strength at 28 days. However, the lowest growth rate of strength was observed in the subsequent 21 days, as shown in Figure 1b.

To further assess the effectiveness of biosilica in geopolymer preparation, geopolymers with a SiO_2/Al_2O_3 molar ratio similar to G_{B30} of 2.7 were synthesised using sodium silicate as an active silicon source. The resulting geopolymer of $G_{S2.7}$ achieved compressive strengths of 33.1 MPa at 7 days and 46.8 MPa at 28 days. While geopolymers prepared using biosilica sources did not match those using commercial sodium silicate in compressive strength, they significantly outperformed pure metakaolin systems (G_{MK}), which exhibited strengths of 1.9 MPa and 3.7 MPa at 7 and 28 days, respectively. This indicates the effectiveness of biosilica as an active silicon source in metakaolin-based geopolymer preparation. These materials are promising for applications in low-strength-demanding areas such as bricks and road repairs.

3.1.2. Influence of Organic Matter

The above studies determined that the optimal mass fraction of DB in metakaolin-based geopolymers was 30 wt% for achieving optimal compressive strength, whereas for DE it was 50 wt%. To investigate the impact of organic matter on strength, calcined forms of DB and DE, referred to as CDB and CDE, respectively, were substituted in geopolymers. The resulting G_{CB30} exhibited compressive strengths of 17.3 MPa at 7 days and 19.3 MPa at 28 days, while G_{CE50} demonstrated strengths of 50.2 MPa and 57.4 MPa, respectively.

In comparison to G_{B30} and G_{E50}, the 28-day strength increases of these samples were 7% and 119%, respectively. The calcination process on biosilica had a significant impact on the compressive strength of the resulting geopolymer products.

The improvement in the effectiveness of the active silicon source with calcination correlates with the organic content in these materials. DE exhibited a Loss on Ignition (LOI) of 20.74%, significantly higher than DB's 9.95%. As a result, the concentration of active silica in the calcined product CDE was notably higher, contributing to a substantial increase in compressive strength at equivalent incorporation levels. These findings underscore the pivotal role of organic content in shaping the properties of geopolymers derived from biosilica sources.

3.2. Compositions

The XRD patterns of geopolymers with different active silica sources, as illustrated in Figure 2, demonstrate that both DB and DE share similar mineral compositions, including chlorite, muscovite, and quartz, with DE additionally displaying albite. The amorphous silica phase present in diatom frustules manifests as a hump peak spanning 17° to 30° (2θ) [31,32]. Notably, the intensity of this peak is significantly lower in DB compared to DE, which indicates a lower concentration of active silica per unit mass in DB. Consequently, geopolymers synthesised from DE exhibited higher compressive strength compared to those from DB at the equivalent mass fractions.

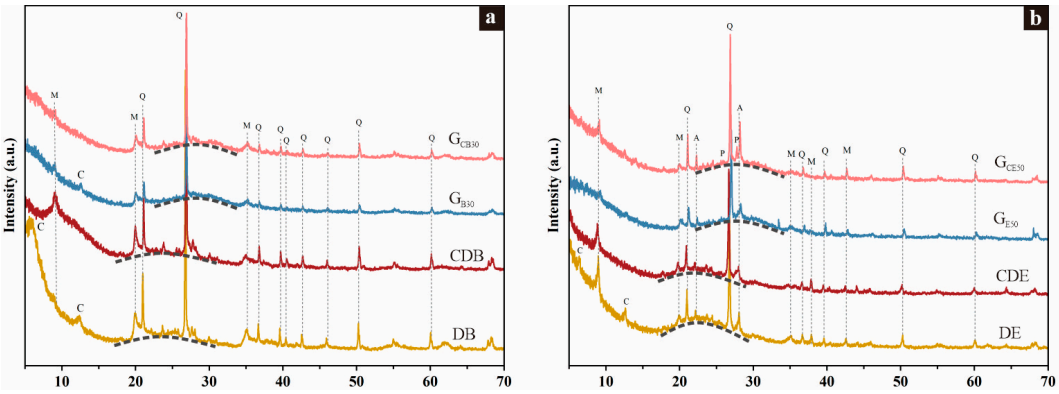


Figure 2. (**a**) XRD patterns of DB, CDB, G_{B30}, and G_{CB30}; (**b**) XRD patterns of DE, CDE, G_{E50}, and G_{CE50}. The XRD patterns of all the geopolymers were obtained at 28 days. (A: albite; C: chlorite; M: muscovite; P: paragonite; Q: quartz).

The hump peaks of the four geopolymers consistently show a shift towards higher angles, typically located at 21° to 33° (2θ), compared to the respective biosilica sources. This shift is a hallmark characteristic of geopolymer gel formation, signifying the depolymerisation and re-condensation of aluminosilicate precursors within the raw materials [33,34]. Furthermore, the other mineral impurity phases including albite, muscovite, and quartz did not participate in the reaction and were filled in the amorphous phase as fine aggregates.

Comparing the spectra of two biosilica sources before and after calcination, minimal changes in mineral compositions were observed. Both CDE and CDB showed characteristic diffractions of minerals that remained largely unchanged post-calcination, except for chlorite. Interestingly, the hump peak area representing amorphous silica exhibited no significant increase. This consistency was similarly noted across the geopolymers studied, whereas calcination was variable. Specifically, there were no significant differences in mineral composition and the quantity of geopolymer gels formed between G_{B30} and G_{CB30}. However, G_{CE50} showed the emergence of a new mineral phase, paragonite [35], while maintaining consistency with G_{E50} in other aspects.

The variations in mineral compositions suggest that while amorphous silica content from biosilica sources plays a critical role in influencing compressive strength, the calcina-

tion process in this study did not enhance strength by increasing this content in biosilica. Additionally, the quantity of geopolymer gels did not obviously show a correlation with strength improvement. The alteration in the chemical composition of the gels due to biosilica calcination may indirectly affect another significant factor that influences strength.

The FTIR spectra of the two biosilica sources, their calcined products, and the corresponding geopolymers are presented in Figure 3. In DB, the vibration band at 1411 cm^{-1} is attributed to symmetric stretching vibrations of carboxyl, which are primary functional groups found in typical organic compounds within fresh diatom biosilica [36]. In DE, the bands at 2926 cm^{-1} and 2853 cm^{-1} correspond to the antisymmetric and symmetric stretching vibrations of methylene, respectively [25]. The band at 1385 cm^{-1} indicates the presence of methyl [37]. These observations suggest a change in the types of the main organic matter. As a commercial product, DB underwent a purification process that resulted in the removal of some of the organic matter; thereby, the variety and content of organic functional groups are not as high as those of DE. Both CDB and CDE show the disappearance of vibration bands associated with organic matter, along with a significant weakening of the hydroxyl group's vibration band near 3700–3600 cm^{-1}. This transformation indicates the removal of organic components and hydroxyl groups during the calcination process.

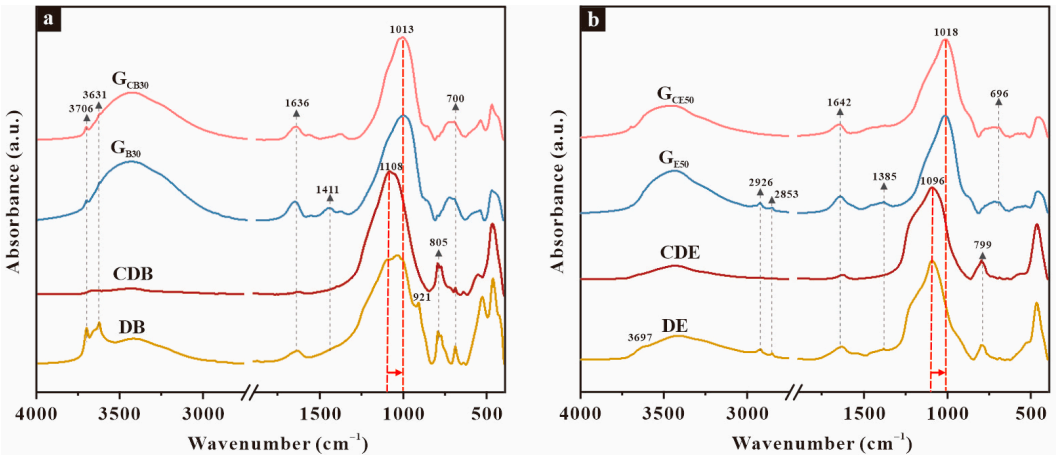


Figure 3. (**a**) FTIR spectra of DB, CDB, G_{B30}, and G_{CB30}; (**b**) FTIR spectra of DE, CDE, G_{E50}, and G_{CE50}. The FTIR spectra of all the geopolymers were obtained at 28 days.

Through the geopolymerisation, the asymmetric stretching vibration of Si-O-(Si, Al) around 1100 cm^{-1} in the biosilica source is replaced by vibration bands around 1015 cm^{-1} in G_{B30}, G_{CB30}, G_{E50}, and G_{CE50} [38,39]. This shift occurs because, in geopolymers, silicon was bound to more aluminium atoms through bridging oxygen than in the structure of frustules, which results in a decrease in the vibrational frequencies of the Si-O-(Si, Al) bond [40–42]. It is noteworthy that organic-related vibration bands are still observable in G_B and G_E, suggesting some organic matter stability in the strong alkaline environment of the activators, possibly forming a barrier against diatom frustule dissolution.

3.3. Microstructure

The processes of mining, grinding, and long-term geologic alteration inevitably result in damage to the structure of diatom frustules [25], which thereby leads to a reduction in their specific surface area [43,44]. This study finds that the specific surface areas of the two types of biosilica sources align with the aforementioned characterisation. The DB, composed of fresh frustules, exhibits a higher specific surface area than the DE, composed of fossilised frustules (Table 4). After calcination, an increase in the specific surface areas of DB and DE is observed. Since no thermally induced phase transition of the mineral impurities in the biosilica sources occurred, as evidenced by the XRD analyses, the removal of organic

matter, namely its conversion to carbon dioxide, is the primary factor contributing to this improvement [45].

Table 4. Specific surface area of biosilica and their calcined products.

Active Silica Source	DB	CDB	DE	CDE
Specific surface area (m^2/g)	27.79	44.84	18.85	25.84

In other studies on the application of diatom frustules, it has often been observed that an increase in the specific surface area of the frustules occurs in conjunction with an increase in the number of active sites, which allows for the enhancement of material properties [18,46]. In the present study, this alteration enhanced the release of active silica by increasing the contact area between the diatom frustules and the activators. As a result, the geopolymers synthesised within calcined biosilica exhibit enhanced compressive strength in comparison to those synthesised with raw biosilica. Nevertheless, this improvement is still constrained by the quantity of amorphous silica present in the biosilica sources, as evidenced by the non-equivalent relationship between the increase in specific surface area and the increase in compressive strength of the products. For instance, while CDB shows a 1.61 times higher specific surface area than DB, G_{CB30} only increases compressive strength by 2.6 MPa compared to G_{B30}. In contrast, despite CDE's modest 37% increase in specific surface area, G_{CE50} demonstrates a 31.2 MPa increase in compressive strength compared to G_{E50}.

Figure 4a,e illustrates the morphology of diatom frustules in biosilica. The fresh frustules in DB with elongated structures are sourced from *Melosira* diatoms, while fossilised frustules in DE exhibiting a disk-like shape with radially symmetrical pores belong to *Coscinodiscus* diatoms [47]. Despite originating from different diatom species, both biosilica types share similar surface characteristics, such as impurities adhering to the frustule surfaces and occasional organic matter wrapping. In fact, the frustule of diatom is a composite of organic matter and silica [48,49], and the silica hydroxyl groups on the surface also facilitate binding with organic matter present in aquatic environments [50]. Thus, the organic covering layer is commonly observed. Following calcination at 750 °C, organic impurities on DB and DE surfaces are removed, revealing clear frustule pore structures of CDB and CDE (Figure 4c,g) without significant structural deformation. Furthermore, a comparison of the DB and DE samples reveals that both contain significant quantities of impurity particles. However, a clear distinction can be observed in the morphology of these particles. They are irregularly shaped as present in DB and can be attributed to mineral impurities. In contrast, DE contains a considerable quantity of fragments resulting from the destruction of the frustules. This observation is in accordance with the previously mentioned point regarding the low integrity of the fossilised frustules.

The microstructural analyses of geopolymers derived from different biosilica sources indicate that the microstructures of G_{B30} and G_{CB30} are less compact than those of G_{E50} and G_{CE50}. This is substantiated by the presence of fish-scale-like fragments in G_{B30} and G_{CB30} (Figure 4b,d), which are indicative of a discontinuous matrix. In contrast, the matrices in G_{E50} and G_{CE50} are observed to be continuous and compact with few cracks and pores (Figure 4f,h). This phenomenon is related to the Si/Al ratio involved in the geopolymerisation. It is generally reported that geopolymers formed under high active Si/Al ratios exhibit excellent mechanical properties [51,52]. EDS analyses indicate that the matrices in G_{E50} and G_{CE50} have higher Si/Al ratios than those in G_{B30} and G_{CB30}, which consequently exhibit higher compressive strengths at both 7 and 28 days.

The aforementioned phenomena did not originate from alterations in the Si/Al ratio inherent to the raw materials; rather, they were a consequence of the proportion of active silica within the total silica content of the raw materials, that is, the efficiency ratio of the silica. At equivalent addition levels, the release of silica monomers was increased due to the enhanced efficiency ratio of silica in biosilica resulting from calcination. This resulted in

the favourable condition of a high Si/Al ratio, which was conducive to geopolymerisation and promoted the formation of geopolymer gels with high degrees of polymerisation. The gels have been observed to possess stable three-dimensional framework structures [52,53]. Conversely, when the efficiency ratio of silica was low, with a correspondingly low release of silica monomers, geopolymerisation occurred under a low Si/Al ratio, resulting in the formation of geopolymer gels with a low degree of polymerisation [54].

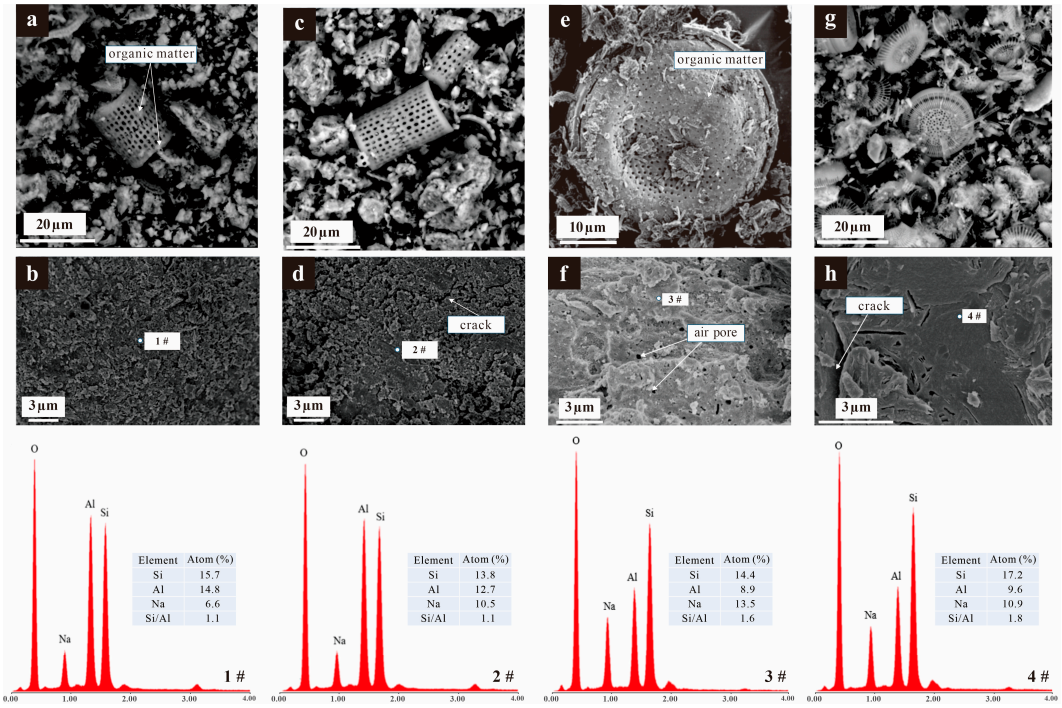


Figure 4. SEM images of (**a**) DB, (**b**) G_{B30}, (**c**) CDB, (**d**) G_{CB30}, (**e**) DE, (**f**) G_{E50}, (**g**) DE, and (**h**) G_{CB50}. The SEM images of the geopolymers and the corresponding EDS analysis results, listed below, were measured at 28 d.

It can be observed that despite the comparable Si/Al ratios of the raw materials, disparities in the efficiency ratio of silica result in variations in the quantity of silica engaged in the geopolymerisation, which in turn influences the mechanical properties of products. It is therefore important to ascertain the efficiency ratio of biosilica as an active silica source for geopolymers. The contents of the amorphous phase and organic matter are useful indicators for this determination. These findings underscore the complex interplay between biosilica properties, calcination effects, and resulting geopolymer characteristics.

4. Conclusions

In conclusion, this study proposes the utilisation of biosilica from both fresh frustules of diatom and fossilised frustules of diatomaceous earth as active silica sources in metakaolin-based geopolymer productions to enhance their sustainability. The research marks a pioneering investigation into the availability of these biosilica sources and their comparative effectiveness. Diatoms demonstrate significant potential for the first time, achieving 28-day compressive strengths of up to 17.9 MPa at a 30% mass fraction, while diatomaceous earth, with a similar silica content, reaches optimal strengths at a 50% addition rate, yielding 26.2 MPa. Although geopolymers prepared from biosilica sources do not exhibit comparable compressive strength to those prepared from commercial sodium silicate, their performance is significantly superior to that of pure metakaolin systems. Consequently, they remain a viable option.

Further analysis of the properties of the biosilica sources with and without organic matter, as well as the microstructure and elemental composition of their geopolymer

products, revealed crucial insights into their performance in geopolymerisation. The following conclusions are drawn:

- The amorphous phase and organic matter present in biosilica are of critical importance in influencing the release of silicon monomers.
- Organic matter in biosilica exhibits chemical stability in strong alkaline environments, hindering the dissolution of frustules, which reduces the release amount of active silica while increasing the presence of impurity particles that need to be cemented.
- Calcination treatment for biosilica effectively removes organic matter, thereby enhancing the efficiency ratio of active silica content.

Overall, this research not only introduces a novel approach to reducing the carbon footprint associated with geopolymers but also highlights the potential of diatoms as a renewable resource. By leveraging biosilica from diatom, this study contributes to advancing sustainable practices in mineral-based materials science.

Author Contributions: Conceptualisation, H.G.; methodology, Z.H. and B.Z.; formal analysis, Z.H.; resources, P.Y.; data curation, Z.H.; writing—original draft preparation, H.G.; writing—review and editing, B.Z., T.Y., T.P. and J.L.; project administration, H.G.; funding acquisition, H.G. and P.Y. All authors have read and agreed to the published version of the manuscript.

Funding: This research was funded by the Guangdong Basic and Applied Basic Research Foundation (Grant No. 2021A1515110941), GDAS' Project of Science and Technology Development (Grant No. 2022GDASZH-2022010104, 2023GDASZH-2023010104), and the National Natural Science Foundation of China (Grant No. 42272043).

Data Availability Statement: The authors confirm that the data supporting the findings of this study are available within the article.

Acknowledgments: We thank the editors and anonymous reviewers for their helpful comments and suggestions.

Conflicts of Interest: The authors declare no conflicts of interest.

References

1. Ren, B.; Zhao, Y.; Bai, H.; Kang, S.; Zhang, T.; Song, S. Eco-friendly geopolymer prepared from solid wastes: A critical review. *Chemosphere* **2021**, *267*, 128900. [CrossRef] [PubMed]
2. Wu, Y.G.; Lu, B.W.; Bai, T.; Wang, H.; Du, F.P.; Zhang, Y.F.; Cai, L.; Jiang, C.; Wang, W.J. Geopolymer, green alkali activated cementitious material: Synthesis, applications and challenges. *Constr. Build. Mater.* **2019**, *224*, 930–949. [CrossRef]
3. Fernández-Jiménez, A.; Palomo, A. 6—Nanostructure/microstructure of fly ash geopolymers. In *Geopolymers*; Provis, J.L., van Deventer, J.S.J., Eds.; Woodhead Publishing: Cambridge, UK, 2009; pp. 89–117. [CrossRef]
4. Zhang, Z.H.; Zhu, H.J.; Zhou, C.H.; Wang, H. Geopolymer from kaolin in China: An overview. *Appl. Clay Sci.* **2016**, *119*, 31–41. [CrossRef]
5. Bai, C.; Shao, J.; Li, X.; Zhang, Z.; Qiao, Y.; Hao, J.; Li, H.; Zheng, T.; Colombo, P. Fabrication and properties of slag-based geopolymer syntactic foams containing hollow glass microspheres. *Mater. Lett.* **2022**, *308*, 131158. [CrossRef]
6. Guo, H.; Yuan, P.; Zhang, B.; Wang, Q.; Deng, L.; Liu, D. Realization of high-percentage addition of fly ash in the materials for the preparation of geopolymer derived from acid-activated metakaolin. *J. Clean. Prod.* **2021**, *285*, 125430. [CrossRef]
7. Duxson, P.; Fernández-Jiménez, A.; Provis, J.L.; Lukey, G.C.; Palomo, A.; van Deventer, J.S.J. Geopolymer technology: The current state of the art. *J. Mater. Sci.* **2007**, *42*, 2917–2933. [CrossRef]
8. Aziz, I.H.; Abdullah, M.M.A.; Yong, H.C.; Ming, L.Y.; Hussin, K.; Surleva, A.; Azimi, E.A. Manufacturing parameters influencing fire resistance of geopolymers: A review. *Proc. Inst. Mech. Eng. Part L J. Mater. Des. Appl.* **2019**, *233*, 721–733. [CrossRef]
9. Glasby, T.; Day, J.; Genrich, R.; Aldred, J. EFC Geopolymer Concrete Aircraft Pavements at Brisbane West Wellcamp Airport. In Proceedings of the Concrete 2015 Conference, Melbourne, Australia, 30 August–2 September 2015.
10. Almutairi, A.L.; Tayeh, B.A.; Adesina, A.; Isleem, H.F.; Zeyad, A.M. Potential applications of geopolymer concrete in construction: A review. *Case Stud. Constr. Mater.* **2021**, *15*, e00733. [CrossRef]
11. Liew, Y.-M.; Heah, C.-Y.; Mohd Mustafa, A.B.; Kamarudin, H. Structure and properties of clay-based geopolymer cements: A review. *Prog. Mater. Sci.* **2016**, *83*, 595–629. [CrossRef]
12. Zhang, Z.; Wang, K.; Mo, B.; Li, X.; Cui, X. Preparation and characterization of a reflective and heat insulative coating based on geopolymers. *Energy Build.* **2015**, *87*, 220–225. [CrossRef]

13. Davidovits, J. 30 Years of successes and failures in geopolymer applications. Market trends and potential breakthroughs. In Proceedings of the Geopolymer 2002 Conference, Melbourne, Australia, 28–29 October 2002; Geopolymer Institute: Melbourne, Australia, 2002.
14. Rashad, A.M. Alkali-activated metakaolin: A short guide for civil Engineer—An overview. *Constr. Build. Mater.* **2013**, *41*, 751–765. [CrossRef]
15. Mejía, J.M.; Mejía de Gutiérrez, R.; Montes, C. Rice husk ash and spent diatomaceous earth as a source of silica to fabricate a geopolymeric binary binder. *J. Clean. Prod.* **2016**, *118*, 133–139. [CrossRef]
16. Bagci, C.; Kutyla, G.P.; Kriven, W.M. Fully Reacted High Strength Geopolymer made with Diatomite as a Fumed Silica Alternative. *Ceram. Int.* **2017**, *43*, 14784–14790. [CrossRef]
17. Fulton, G.P.; Ebrary, I. *Diatomaceous Earth Filtration for Safe Drinking Water*; American Society of Civil Engineers: Reston, VA, USA, 2000.
18. Danil de Namor, A.F.; El Gamouz, A.; Frangie, S.; Martinez, V.; Valiente, L.; Webb, O.A. Turning the volume down on heavy metals using tuned diatomite. A review of diatomite and modified diatomite for the extraction of heavy metals from water. *J. Hazard. Mater.* **2012**, *241–242*, 14–31. [CrossRef] [PubMed]
19. Degirmenci, N.; Yilmaz, A. Use of diatomite as partial replacement for Portland cement in cement mortars. *Constr. Build. Mater.* **2009**, *23*, 284–288. [CrossRef]
20. Ergün, A. Effects of the usage of diatomite and waste marble powder as partial replacement of cement on the mechanical properties of concrete. *Constr. Build. Mater.* **2011**, *25*, 806–812. [CrossRef]
21. Phoo-Ngernkham, T.; Chindaprasirt, P.; Sata, V.; Sinsiri, T. High calcium fly ash geopolymer containing diatomite as additive. *Indian J. Eng. Mat. Sci.* **2013**, *20*, 310–318.
22. Posi, P.; Lertnimoolchai, S.; Sata, V.; Phoo-ngernkham, T.; Chindaprasirt, P. Investigation of properties of lightweight concrete with calcined diatomite aggregate. *KSCE J. Civ. Eng.* **2014**, *18*, 1429–1435. [CrossRef]
23. Li, J.; Jin, Q.; Zhang, W.; Li, C.; Monteiro, P.J.M. Microstructure and durability performance of sustainable cementitious composites containing high-volume regenerative biosilica. *Resour. Conserv. Recycl.* **2022**, *178*, 106038. [CrossRef]
24. Sharma, N.; Simon, D.P.; Diaz-Garza, A.M.; Fantino, E.; Messaabi, A.; Meddeb-Mouelhi, F.; Germain, H.; Desgagné-Penix, I. Diatoms Biotechnology: Various Industrial Applications for a Greener Tomorrow. *Front. Mar. Sci.* **2021**, *8*, 636613. [CrossRef]
25. Jiang, W.; Luo, S.; Liu, P.; Deng, X.; Jing, Y.; Bai, C.; Li, J. Purification of biosilica from living diatoms by a two-step acid cleaning and baking method. *J. Appl. Phycol.* **2014**, *26*, 1511–1518. [CrossRef]
26. Lutynski, M.; Sakiewicz, P.; Lutynska, S. Characterization of Diatomaceous Earth and Halloysite Resources of Poland. *Minerals* **2019**, *9*, 670. [CrossRef]
27. Xun, B.; Jiang, Y.; Yang, D.; Shi, X. Carbonization Treatment of Diatomite with High Ignition Loss and Reinforcement of Natural Rubber. *Chem. J. Chin. Univ.* **2011**, *32*, 1617–1621.
28. Guo, H.; Zhang, B.; Deng, L.; Yuan, P.; Li, M.; Wang, Q. Preparation of high-performance silico-aluminophosphate geopolymers using fly ash and metakaolin as raw materials. *Appl. Clay Sci.* **2021**, *204*, 106019. [CrossRef]
29. Pereira, D.G.; Afonso, A.; Medeiros, F.M. Overview of Friedman's Test and Post-hoc Analysis. *Commun. Stat.—Simul. Comput.* **2015**, *44*, 2636–2653. [CrossRef]
30. Brunauer, S.; Emmett, P.H.; Teller, E. Adsorption of Gases in Multimolecular Layers. *J. Am. Chem. Soc.* **1938**, *60*, 309–319. [CrossRef]
31. Yu, W.B.; Yuan, P.; Liu, D.; Deng, L.L.; Yuan, W.W.; Tao, B.; Cheng, H.F.; Chen, F.R. Facile preparation of hierarchically porous diatomite/MFI-type zeolite composites and their performance of benzene adsorption: The effects of NaOH etching pretreatment. *J. Hazard. Mater.* **2015**, *285*, 173–181. [CrossRef] [PubMed]
32. Curtis, N.J.; Gascooke, J.R.; Johnston, M.R.; Pring, A. A Review of the Classification of Opal with Reference to Recent New Localities. *Minerals* **2019**, *9*, 299. [CrossRef]
33. Karuppaiyan, J.; Jeyalakshmi, R.; Kiruthika, S.; Wadaan, M.A.; Khan, M.F.; Kim, W. A study on the role of surface functional groups of metakaolin in the removal of methylene blue: Characterization, kinetics, modeling and RSM optimization. *Environ. Res.* **2023**, *226*, 115604. [CrossRef]
34. Duxson, P.; Provis, J.L.; Lukey, G.C.; Separovic, F.; van Deventer, J.S.J. ^{29}Si NMR study of structural ordering in aluminosilicate geopolymer gels. *Langmuir* **2005**, *21*, 3028–3036. [CrossRef]
35. Obiora, S.C.; Umeji, A.C. Petrographic evidence for regional burial metamorphism of the sedimentary rocks in the Lower Benue rift. *J. Afr. Earth Sci.* **2004**, *38*, 269–277. [CrossRef]
36. Gale, D.K.; Gutu, T.; Jiao, J.; Chang, C.-H.; Rorrer, G.L. Photoluminescence Detection of Biomolecules by Antibody-Functionalized Diatom Biosilica. *Adv. Funct. Mater.* **2009**, *19*, 926–933. [CrossRef]
37. Rodriguez-Vidal, F.J.; Ortega-Azabache, B.; Gonzalez-Martinez, A.; Bellido-Fernandez, A. Comprehensive characterization of industrial wastewaters using EEM fluorescence, FT-IR and ^{1}H NMR techniques. *Sci. Total Environ.* **2022**, *805*, 150417. [CrossRef]
38. Sitarz, M. The structure of liquation silico-phosphate glasses. *J. Mol. Struct.* **2008**, *887*, 229–236. [CrossRef]
39. Zhang, B.; Guo, H.; Yuan, P.; Deng, L.; Liu, D. Novel acid-based geopolymer synthesized from nanosized tubular halloysite: The role of precalcination temperature and phosphoric acid concentration. *Cem. Concr. Compos.* **2020**, *110*, 103601. [CrossRef]

40. Zhang, B.; Yuan, P.; Guo, H.; Deng, L.; Li, Y.; Li, L.; Wang, Q.; Liu, D. Effect of curing conditions on the microstructure and mechanical performance of geopolymers derived from nanosized tubular halloysite. *Constr. Build. Mater.* **2020**, *268*, 121186. [CrossRef]
41. Fernández-Jiménez, A.; Palomo, A. Mid-infrared spectroscopic studies of alkali-activated fly ash structure. *Microporous Mesoporous Mater.* **2005**, *86*, 207–214. [CrossRef]
42. Rees, C.A.; Provis, J.L.; Lukey, G.C.; van Deventer, J.S.J. Attenuated total reflectance Fourier transform infrared analysis of fly ash geopolymer gel aging. *Langmuir* **2007**, *23*, 8170–8179. [CrossRef]
43. Wang, Y.; Cai, J.; Jiang, Y.; Jiang, X.; Zhang, D. Preparation of biosilica structures from frustules of diatoms and their applications: Current state and perspectives. *Appl. Microbiol. Biotechnol.* **2013**, *97*, 453–460. [CrossRef]
44. Huang, J.; Wu, B.; Lyu, S.; Li, T.; Han, H.; Li, D.; Wang, J.-K.; Zhang, J.; Lu, X.; Sun, D. Improving the thermal energy storage capability of diatom-based biomass/polyethylene glycol composites phase change materials by artificial culture methods. *Sol. Energy Mater. Sol. Cells* **2021**, *219*, 110797. [CrossRef]
45. Umemura, K.; Noguchi, Y.; Ichinose, T.; Hirose, Y.; Kuroda, R.; Mayama, S. Diatom Cells Grown and Baked on a Functionalized Mica Surface. *J. Biol. Phys.* **2008**, *34*, 189–196. [CrossRef] [PubMed]
46. Chen, K.; Li, C.; Shi, L.; Gao, T.; Song, X.; Bachmatiuk, A.; Zou, Z.; Deng, B.; Ji, Q.; Ma, D. Growing three-dimensional biomorphic graphene powders using naturally abundant diatomite templates towards high solution processability. *Nat. Commun.* **2016**, *7*, 13440. [CrossRef] [PubMed]
47. Zhang, D.; Wang, Y.; Zhang, W.; Pan, J.; Cai, J. Enlargement of diatom frustules pores by hydrofluoric acid etching at room temperature. *J. Mater. Sci.* **2011**, *46*, 5665–5671. [CrossRef]
48. Nakajima, T.; Volcani, B.E. 3,4-Dihydroxyproline: A New Amino Acid in Diatom Cell Walls. *Science* **1969**, *164*, 1400–1401. [CrossRef] [PubMed]
49. Nakajima, T.; Volcani, B.E. ϵ-N-trimethyl-L-δ-hydroxylysine phosphate and its nonphosphorylated compound in diatom cell walls. *Biochem. Biophys. Res. Commun.* **1970**, *39*, 28–33. [CrossRef]
50. Loucaides, S.; Behrends, T.; Van Cappellen, P. Reactivity of biogenic silica: Surface versus bulk charge density. *Geochim. Cosmochim. Acta* **2010**, *74*, 517–530. [CrossRef]
51. Rozek, P.; Krol, M.; Mozgawa, W. Geopolymer-zeolite composites: A review. *J. Clean. Prod.* **2019**, *230*, 557–579. [CrossRef]
52. Silva, P.D.; Sagoe-Crenstil, K.; Sirivivatnanon, V. Kinetics of geopolymerization: Role of Al_2O_3 and SiO_2. *Cem. Concr. Res.* **2007**, *37*, 512–518. [CrossRef]
53. Sagoe-Crentsil, K.; Weng, L. Dissolution processes, hydrolysis and condensation reactions during geopolymer synthesis: Part II. High Si/Al ratio systems. *J. Mater. Sci.* **2007**, *42*, 3007–3014. [CrossRef]
54. Weng, L.; Sagoe-Crentsil, K. Dissolution processes, hydrolysis and condensation reactions during geopolymer synthesis: Part I—Low Si/Al ratio systems. *J. Mater. Sci.* **2007**, *42*, 2997–3006. [CrossRef]

Disclaimer/Publisher's Note: The statements, opinions and data contained in all publications are solely those of the individual author(s) and contributor(s) and not of MDPI and/or the editor(s). MDPI and/or the editor(s) disclaim responsibility for any injury to people or property resulting from any ideas, methods, instructions or products referred to in the content.